



Research paper

Enhancement in site-specific delivery of carvacrol for potential treatment of infected wounds using infection responsive nanoparticles loaded into dissolving microneedles: A proof of concept study

Maria Mir^{a,b}, Andi Dian Permana^{b,c}, Naveed Ahmed^a, Gul Majid Khan^a, Asim ur Rehman^{a,*}, Ryan F. Donnelly^{b,*}

^a Department of Pharmacy, Faculty of Biological Sciences, Quaid-i-Azam University, Islamabad 45320, Pakistan

^b School of Pharmacy, Medical Biology Centre, Queen's University Belfast, 97 Lisburn Road, Belfast BT9 7BL, United Kingdom

^c Department of Pharmaceutics, Faculty of Pharmacy, Hasanuddin University, Makassar 90234, Indonesia

ARTICLE INFO

Keywords:

Carvacrol
Nanoparticles
Wound
Microneedles
Methicillin resistant *Staphylococcus aureus* (MRSA)
Pseudomonas aeruginosa

ABSTRACT

Chronic wound infections have become a challenging problem due to escalating antibiotic resistance and lack of viable delivery approaches. Carvacrol (CAR) has been reported to be effective against multidrug resistant pathogens. In this study, CAR was formulated into a site-specific nanoparticle (NP) delivery system using poly (caprolactone) (PCL) to achieve a sustained antimicrobial effect at infection sites. These NPs were further incorporated into dissolving microneedles (MNs) to facilitate painless application and overcome the necrotic tissue barrier which hinders drug penetration into wound bed. The release study exhibited significantly higher release of CAR from PCL NPs in the presence of bacteria, highlighting its potential for on-demand delivery. Moreover, encapsulation of CAR in PCL NPs resulted in 2–4 fold increase in its antimicrobial activity. Dermatokinetic studies revealed that CAR-PCL NPs-MNs were able to enhance skin retention of CAR after 24 h ($83.8 \pm 5.15\%$), compared to free CAR-MNs ($7.3 \pm 2.04\%$). Importantly, this novel approach exhibited effective antimicrobial activity in an *ex-vivo* wound model. Hence, these findings have proven the concept that loading of CAR into this advanced MNs platform can lead to sustained antimicrobial effect at desired site and may provide a novel effective approach for treatment of infected wounds. However, further studies must be conducted to investigate *in-vivo* efficacy of the developed system in an appropriate infection model.

1. Introduction

Management of infected chronic wounds has become a major concern for public health and medical practices worldwide, due to increasing prevalence of chronic wounds, escalating antimicrobial resistance and lack of viable methods for delivery of antimicrobials [1]. Chronic wounds include diabetic foot ulcers, venous ulcers and pressure ulcers and are commonly present in the older patients with either diabetes mellitus or vascular diseases or surgeries [2]. The annual cost for management of patients with chronic wounds in US is found to be an excess of 25 billion US\$, hence, there is a pressing need for novel antimicrobials and delivery approaches [3]. Wounds are vulnerable to polymicrobial infections, which impair the healing process of wounds, demanding the additional health care costs [4]. Although a variety of pathogens are involved, the most commonly-isolated pathogens include *Staphylococcus aureus*, and *Pseudomonas aeruginosa* [4,5]. With the

emergence of resistance of these pathogens to commonly used antibiotics, including the aminoglycosides, macrolides, fluoroquinolones and tetracyclines [6,7], it is becoming challenging to find safe, simple and effective treatment options for these infections [8]. More recently, studies have reported the emergence of resistance to linezolid, vancomycin and daptomycin [9,10]. With limited treatment options available, there is a requirement for identification of alternative agents for management of these often life-threatening infections [11].

Essential oils and their bioactive molecules have been reported to exhibit antimicrobial properties against a range of Gram-positive and Gram-negative pathogenic bacteria [12,13]. Among these, carvacrol (CAR), 5-isopropyl-2-methylphenol, a monoterpenoid phenolic compound, and the principal component of many plant essential oils, has manifested antimicrobial potential against a broad range of resistant pathogens [14]. CAR acts in multiple ways to kill the pathogens making the development of resistance difficult. Specifically, it causes disruption

* Corresponding authors.

E-mail addresses: arehman@qau.edu.pk (A.u. Rehman), r.donnelly@qub.ac.uk (R.F. Donnelly).

<https://doi.org/10.1016/j.ejpb.2019.12.008>

Received 26 October 2019; Received in revised form 14 December 2019; Accepted 16 December 2019

Available online 27 December 2019

0939-6411/ © 2019 The Author(s). Published by Elsevier B.V. This is an open access article under the CC BY license (<http://creativecommons.org/licenses/by/4.0/>).

of cell membranes and proton gradient, inhibition of ATP synthesis and efflux pumps, suppression of two essential virulence factors, namely enterotoxin and coagulase, and inhibition of quorum sensing and bio-film formation [15,16]. Furthermore, it has been reported to exhibit wound healing properties [17]. In spite of the promising antimicrobial profile of CAR, its direct application still encounters challenges owing to its permeability, that leads to poor skin retention, requiring frequent applications. Therefore, development of an optimized delivery system is required to achieve sustained antimicrobial effect at the site of infection [18,19]. Additionally, site-specific delivery of antimicrobials helps to reduce the possibility of resistance by minimizing their exposure to the only pathogens at the infection site [20].

To selectively deliver antibiotics to the site of infection, various nanocarrier systems have been investigated utilizing the unique microenvironment of infection site, including lower pH [21], higher temperature [22], surface proteins [23], secreted bacterial toxins [24] and higher expression of bacterial enzymes [25]. As triggering motifs for infection responsive delivery, enzymes are the most promising ones, as enzymatic reactions are more efficient and selective under mild conditions and are also involved in the bacterial metabolic and pathological processes. Importantly, specific enzymes are actively produced by resistant strains [26]. Xiong et al. [27] has recently reported the chemical synthesis of bacterial lipase-sensitive poly (ϵ -caprolactone) (PCL) nanogel for specific delivery of antimicrobials to infection sites. Thus, production of lipase at infection sites may be utilized to selectively deliver antimicrobials to the desired site and may prove an effective, safe treatment approach.

The selection of the final dosage form for delivery of drug cargos; in terms of its suitability for application and patient acceptability is very important. Infected wounds are being treated either locally or systemically. However, upon systemic administration, accumulation of antimicrobials does not occur at the desired site of infection due to avascular nature of majority of the wounds [28]. Hence, local delivery of antimicrobial agents may often be preferred over systemic delivery to localize the drug at infection site. However, the conventional dosage forms like solutions and gels have several limitations including; poor retention at the site leading to inaccurate dosing, requiring frequent applications, and inability to overcome the necrotic/hyperkeratotic tissue barrier (present in chronic wounds) leading to poor penetration into the wound bed [17,29,30]. Moreover, conventional dressings often result in problems related with their removal as these may cause trauma by stripping off newly formed epidermis [31,32]. Considering the potential of microneedles (MNs) to successfully penetrate through necrotic tissue barrier, (avoiding the requirement of surgical debridement before application; an approach being practiced in clinics), facilitating the painless, direct and rapid delivery of accurate doses of drug cargos into the wound beds; MNs were considered to be the optimum choice for delivery of designed NPs to the chronic wounds [33–35].

Herein, we report for the first time the development of NPs laden with CAR for potential treatment of wound infections. NPs were fabricated from the bacterial lipase-sensitive poly(ϵ -caprolactone) polymer employing simple nanoprecipitation approach, to avoid complex chemical synthesis. It is anticipated that encapsulation of CAR within NPs, would prevent nonspecific release, while providing the opportunity to selectively deliver CAR to infected tissue through NPs degradation by bacterial lipases at infection sites. For effective delivery of designed NPs to infected chronic wounds, these were further loaded into the dissolving MN arrays, followed by optimization of MNs design and comprehensive *in-vitro* characterization. In order to investigate the concept that loading of CAR into PCL NPs can prolong the availability of CAR in skin layers, in addition to improving its antibacterial activity, the following studies were conducted; *ex-vivo* dermatokinetic profiling, and antimicrobial efficacy studies in an *ex-vivo* porcine skin infection model. This is the first reported study utilizing this approach for enhancement of local delivery of CAR.

2. Materials and methods

2.1. Materials

Poly(caprolactone)(PCL) (MW 14,000 Da), carvacrol (> 98% purity), Poloxamer® 407, and acetone (> 99.5%) were all procured from Sigma-Aldrich, Hamburg, Germany. Gantrez® S-97, which is poly (methylvinylether/maleic acid) (MW 1,500,000 Da) was a gift from Ashland, Kidderminster, UK. Poly (vinyl pyrrolidone) (PVP) (MW 29,000–32,000 Da) was obtained from Ashland Industries Europe GmbH, Schaffhausen, Switzerland. Poly (vinyl alcohol) (PVA) (MW 31,000–50,000 Da) was purchased from Sigma-Aldrich Chemie GmbH, Steinheim, Germany. All reagents used were of analytical grade.

2.2. Preparation of nanoparticles

Blank and CAR-PCL NPs were prepared using a nanoprecipitation method. Briefly, PCL (10 mg/mL) was dissolved in 4 mL of acetone with mild heating (37–40 °C), followed by the addition of CAR (5 mg/mL) in this polymer solution. This organic phase was then added dropwise into 12 mL of milli-Q water containing Poloxamer®407 (0.5% w/v) under homogenization at 6500 rpm (Silent Crusher M Homogenizer from Heidolph Instruments, Schwabach, Germany). The organic solvent was evaporated at room temperature with magnetic stirring for 1 h and the resultant dispersion was subjected to centrifugation (Hermle Labortechnik GmbH, Z-206A, Siemensstr.25 D-78564 Wehingen, Germany) for 30 min at 13,500 rpm and 4 °C. Supernatant was removed and the sediment (consisting of NPs) was washed with milli-Q water twice using the same centrifugation conditions. PVP (29–32 kDa) was then added as cryoprotectant into the collected sediment in the concentration range of 0.5% to 2% w/v and formulation was frozen overnight at –80 °C, before lyophilization (Alpha 1–2 LD plus, Christ, Osterode, Germany). Blank PCL NPs were also formulated as above, without the addition of CAR in the organic phase. Additionally, fluorescent dye (Nile red) loaded NPs (NR-PCL NPs) were also prepared following the same protocol as for CAR-PCL NPs, for the purpose of fluorescence imaging.

2.3. Characterization of nanoparticles

Both the blank and CAR-PCL NPs were characterized in terms of particle size, polydispersity index (PDI) and zeta potential (ZP) using NanoBrook Omni particle sizer and zeta potential analyzer (Brookhaven, New York, NY, USA) at 25 ± 2 °C, after diluting 20 μ L of NPs up to 2 mL with double distilled water. To determine the entrapment efficiency (EE) of CAR-PCL NPs, prepared formulation was centrifuged at 13,500 rpm, 4 °C for 30 min to separate the CAR-PCL NPs from free drug. After collection, filtered supernatant (through 0.45 μ m syringe filter) was analyzed for CAR content using the analytical method provided in Supplementary information Section S1. Eq. (1) was used to determine EE:

$$\text{Entrapment efficiency (EE) \%} = \frac{\text{Total CAR added} - \text{Free CAR in supernatant}}{\text{Total CAR added}} * 100 \quad (1)$$

2.4. Culture of bacterial strains

Lipase-secreting bacteria used in this study including; *Staphylococcus aureus* (NCTC® 10788), *Staphylococcus aureus* (ATCC® 33593TM), *Staphylococcus aureus* [MW2] (ATCC® BAA-1707TM), *Pseudomonas aeruginosa* (ATCC® 9027) and *Pseudomonas aeruginosa* [PAO1] (ATCC®BAA- 47), were directly purchased from LGC Standards, Middlesex, UK. All the strains were maintained at 4°C and sub-cultured at regular intervals on fresh media. Before each antimicrobial assay, S.

aureus (NCTC® 10788) and MRSA (ATCC® 33593TM and ATCC® BAA-1707TM) strains were cultured overnight in Mueller Hinton broth (MHB) and *Pseudomonas aeruginosa* strains (ATCC® 9027 and ATCC®BAA- 47) in Luria-Bertani broth (LBB), at 37 °C, 100 rpm and then resulting cultures were centrifuged at 3000 rpm for 25 min to get pellet. The obtained pellet was resuspended in fresh MHB/LBB and optical density OD₅₅₀ of bacterial suspensions was set to 1.5×10^8 CFU/mL (precise bacterial count was determined by plating the diluted suspensions on Mueller Hinton agar (MHA) and Luria-Bertani agar (LBA) plates). Working inoculums were established by multistep dilutions with MHB/LBB to obtain final concentrations of 2.0×10^5 CFU/mL.

2.5. In-vitro release study of CAR-PCL NPs in bacterial cultures

To evaluate the bacterial enzyme responsive release behavior of CAR-PCL NPs, release studies were conducted in both the presence and absence of lipase-secreting bacteria [27]. For this purpose, NPs were dispersed in 20 mL of bacterial cultures (optical density OD₅₅₀ was set to 0.1 following the same way mentioned in Section 2.4) in McCartney vials, and placed in an orbital shaker at 100 rpm, 37 ± 1 °C temperature. Samples (500 µL volumes) were taken at pre-determined time points (0.5, 2, 4, 6, 8, 12 and 24 h) and ultra-filtered using Millipore's Amicon Ultra-0.5 centrifugal filters. The filtrate was collected and analyzed using the analytical method detailed in Supplementary information Section S1. Results were obtained in triplicate (n = 3) and expressed as mean \pm standard deviation (SD). Cumulative % release was determined through Eq. (2):

$$\text{Cumulative release (\%)} = \text{Ct. Vo} + \sum_{i=0}^{t-1} \text{Vi} * 100 / \text{CAR (initial conc)} \quad (2)$$

where Vo = Initial broth volume, Vi = Volume of sample taken, Ct = CAR concentration in each sample estimated through HPLC

The mechanism of release of CAR from CAR-PCL NPs was studied by applying different mathematical models including; Zero-order, First-order, Hixson-Crowell, Higuchi and Korsmeyer-Peppas on *in-vitro* data using DD Solver software. Significant differences between multiple groups were determined through one-way analysis of variance (ANOVA) using GraphPad Prism® software version 5.03 (GraphPad Software, San Diego, CA, USA).

2.6. Antimicrobial assays

2.6.1. Determination of minimum inhibitory concentration and minimum bactericidal concentration

Minimum inhibitory concentrations (MICs) of CAR, blank PCL NPs and CAR-PCL NPs were determined against both Gram-positive and Gram-negative strains through microtiter broth dilution method using 96-well plates as previously described [36]. Two-fold serial dilutions of CAR, blank PCL NPs and CAR-PCL NPs were made with broth (MHB for *S. aureus* strains and LBB for *Pseudomonas aeruginosa* strains) to achieve final concentrations ranging from 2.5 mg/mL to 0.039 mg/mL. 100 µL of each bacterial suspension was inoculated to all wells to obtain final bacterial concentration of 2.0×10^5 CFU/mL. Broth (MHB/LBB) with inoculum without any antibacterial agent was included as positive control. The inoculated microplates were incubated at 37 °C for 24 h. MIC was estimated as the minimum concentration of CAR, blank PCL NPs and CAR-PCL NPs completely inhibiting the visible growth of bacteria following overnight incubation.

To estimate minimum bactericidal concentration (MBC), 20 µL from each well exhibiting no visible growth was cultured on MHA/LBA plates and incubated at 37 °C for 24 h. The minimum concentration of CAR and CAR-PCL NPs causing > 99.9% inhibition of bacterial growth was considered as the MBC. Three inter-day and intra-day replications

were performed for both MICs and MBCs determinations.

2.6.2. Time kill assay

Killing kinetics of CAR and CAR-PCL NPs against lipase-secreting Gram-positive and Gram-negative strains was evaluated following the previously reported method [37]. Briefly, the concentration of test strains was set to 2.0×10^5 CFU/mL following the same way mentioned in Section 2.4. Bacterial suspensions were then treated with CAR and CAR-PCL NPs in concentrations equivalent to their MICs and $2 \times$ MICs, followed by incubation at 37 °C. Samples from the cultures were withdrawn at 0, 4, 6, 8, 12, 18 and 24 h incubation time points and inoculated on MHA/LBA plates with appropriate dilutions with sterile fresh broth. Plates were analysed for viable CFUs after 24 h of incubation at 37°C. A control was also run under the same conditions (without CAR and CAR-PCL NPs) for growth of test strains at all time points. The CFUs retrieved post-treatment were compared for both CAR and CAR-PCL NPs and plotted as the log CFU/mL against post-treatment time. The relationship between viable cell count and time was determined through time-kill curve.

2.7. Fabrication of dissolving MN arrays

In order to fabricate CAR-PCL NPs in dissolving MN arrays with optimum characteristics, various designs and casting methods were tested, as described in Table 2. For micromolding of MN arrays, master-templated (16×16 needle density, cuboidal in shape, 850 µm in height with base width of 300 µm and interspacing of 100 µm) silicone micromolds (F1 to F7) and laser-engineered (19×19 needle density, conical in shape, 600 µm in height with base width of 300 µm and interspacing of 50 µm) silicone micromolds (F8-F10) were used. A two-step casting method was investigated with different dissolving MN formulations. For the purpose, initially, the lyophilized CAR-PCL NPs were mixed with PVA/PVP hydrogels until homogenous. In the first step, aqueous blends of CAR-PCL NPs/polymer gels (100 mg) were poured into MN molds using a syringe and placed in a positive pressure chamber (a pressure of 3–4 bar) for 5 min to fill the cavity of the molds. Subsequently, molds were taken from the pressure chamber, excess of formulation removed and positive pressure repeated for 15 min, followed by 24 h of drying in a temperature controlled room at 19°C. In a second step, PVA/PVP hydrogels were poured into the 24 h-dried molds and subjected to a positive pressure of 3–4 bars for 15 min, followed by 48 h drying at 19°C. Upon drying, MN arrays were demolded and assessed for needle formation and mechanical strength. For laser-engineered conical silicone molds (F8-F10) the same fabrication protocol was followed, with the exception of use of centrifugation (5000 rpm for 15 min) in place of compression in a pressure chamber. Various formulations used to fabricate MN arrays (F1-F10) and little modifications done in this method (F1-F7), to obtain an optimum formulation, are given in Table 2.

To use as a control in all dermatokinetic and microbiology studies, free CAR loaded MN arrays were also fabricated. To prepare CAR loaded MN arrays, one step casting method was used. Various polymer blends with different concentrations of CAR were prepared as potential matrices for fabrication of MN arrays (Table S2). These aqueous blends (500 mg) were poured into the laser-engineered silicone molds (19×19 needle density, conical in shape, 600 µm in height with base width of 300 µm and interspacing of 50 µm) and subjected to centrifugation for 15 min at 5000 rpm followed by drying in the temperature controlled room at 19 °C for 48 h. Upon drying, the sidewalls formed by the molding process (only formed by the centrifuge process) were removed using a heated blade and subsequently, inspected using a Leica EZ4D digital light microscope (Leica Microsystems, Milton Keynes, UK) and scanning electron microscope (SEM) TM3030 (Hitachi, Krefeld, Germany). In order to locate the NPs in needles, NR-PCL NPs loaded MN arrays were also fabricated, following the same method as employed for CAR-PCL NPs loaded MN arrays.

2.8. Evaluation of mechanical strength and insertion properties of MN arrays

MN arrays were evaluated for their mechanical strength and insertion properties using a TA-XT2 Texture Analyzer (Stable Microsystems, Haslemere, UK), as described previously [38]. Briefly, MN arrays were attached to the moveable cylindrical probe (5 cm in length, 1.5 cm² cross-sectional areas) of the Texture Analyzer and the probe was set to move downward at a rate of 1.19 mm/s. A 32 N force per array was applied at defined rate for 30 s to compress the MN arrays against a flat metal block of dimensions 9.2 × 5.2 cm [39]. The Leica EZ4D digital microscope (Leica Microsystems, Milton Keynes, UK) was used to visualize the MN arrays before and after application of the compression load. The ruler function of ImageJ® software (US National Institutes of Health, Bethesda, Maryland, USA) was used to measure the heights of individual MNs before and after testing, in order to calculate the percentage height reduction using equation (3).

$$\% \text{Compression} = \frac{H_{BC} - H_{AC}}{H_{BC}} \times 100 \quad (3)$$

where H_{BC} is height before compression and H_{AC} is height after compression.

In order to determine the MN insertion properties, Parafilm M® (Bemis Company Inc, Soignies, Belgium) were used as a skin simulant insertion model, as developed by Larrañeta et al. [39] in order to avoid the dissolution of needles by skin tissue. Briefly, Parafilm M® was folded into eight layers (≈ 1 mm thickness) and MN arrays were inserted using the Texture Analyzer and the same conditions mentioned above. Following this, the MN arrays were removed from the Parafilm M® layers and the number of holes created in each layer was counted using the digital microscope. Images of the inserted MN arrays in Parafilm M® model were also recorded using an EX1301 optical coherence tomography (OCT) microscope (Michelson Diagnostics Ltd., Kent, UK).

2.9. In-skin dissolution of MN arrays

To investigate dissolution kinetics of the developed MN arrays, neonatal porcine skin was used as a model, owing to its structural similarity with human skin [40]. For the purpose, full thickness skin was excised from abdominal part of stillborn piglets (within 24 h of post-mortem) and stored at –20 °C until use. Before performing dissolution studies, the skin was thawed in PBS pH 7.4 at 37 °C and carefully shaved using a disposable razor. The skin was then dried with tissue paper and placed on a sheet (500 μm-thick) of dental wax (An ut ex®, Kemdent Works, Swindon, UK) for support. Subsequently, MN arrays were inserted into the skin manually using thumb pressure for 30 s. To determine the dissolution rate, MN arrays were removed from the skin at defined time points and observed under digital microscope.

2.10. Calculation of drug content in MN arrays

To determine the CAR content in bilayer MN arrays, only needles were removed carefully from the baseplate using a scalpel and dissolved in PBS (pH 7.4). Following this, acetone was added for the disruption of NPs. After dissolving NPs in acetone by vortexing, the resultant dispersion was then centrifuged at 14,000 rpm for 10 min and amount of CAR was quantified in the supernatant using HPLC after making appropriate dilutions with PBS. To determine the CAR content localized in the needles of single layer CAR loaded MN arrays, initially, baseplates were fabricated using the optimized formulation, so that density of the formulation can be calculated. The CAR amount in the needles was calculated using Eq. (4) [41]:

$$\text{Drug in the MN tips: } N \times (h \cdot a^2) \cdot \rho \cdot [\text{Drug}] / 3 \quad (4)$$

where N = Number of needles (19 × 19 = 361), a^2 = Width of base of the needles (0.3 mm), h = Height of the needles (0.6 mm), ρ = density of the dry formulation, and $[\text{Drug}]$ = Concentration of CAR in dry

formulation.

2.11. Particle size determination after loading into MN arrays

Particle size and PDI of CAR-PCL NPs was measured after loading into the MN arrays. For the purpose, MN arrays were dissolved in 15 mL of PBS (pH 7.4) and then small aliquots of the resultant suspension was diluted up to 100 times with distilled water before measuring the particle size using the NanoBrook Omni particle sizer (Brookhaven, New York, NY, USA).

2.12. Ex-vivo dermatokinetic studies

Dermatokinetic and permeation studies were performed with free CAR loaded MN arrays (coded as CAR-MNs) and bilayer CAR-PCL NPs loaded MN arrays containing NPs only in the needles (coded as CAR-PCL NPs-MNs). To investigate the dermatokinetic profile, a previously reported method was employed, using full thickness abdominal neonatal porcine skin [42]. The skin samples were prepared as described in Section 2.9 and placed in the donor compartment of Franz cells, having an area of 1.76 cm² for diffusion. MN arrays were applied to the skin using plunger pressure for 30 s followed by the application of a cylindrical metal mass (mass 5.0 g, diameter 11 mm) to avoid slippage of MN arrays from the skin. PBS (pH 7.4) was added in the receiving compartment and maintained at 37 ± 1 °C temperature with 600 rpm stirring. Both the sampling arm and donor compartment were wrapped with Parafilm M®. CAR-MNs and CAR-PCL NPs-MNs were removed after 30 min of application; skin was cleansed with deionized water and set back to the donor compartment. Samples were taken from both the donor (skin samples) and receiving compartments at pre-determined time intervals; 0.5, 1, 2, 4, 6, 8 and 24 h, for dermatokinetic analysis and estimation of permeation of CAR respectively. In order to process the skin samples, biopsy was performed using a biopsy punch (5 mm diameter) (Stiefel, Middlesex, UK) to collect required skin sections. The skin was then added into glass tubes and heated at 60 °C in a water bath for 2–3 min. Epidermis was further separated manually from the dermal layers using tweezers. Thereafter, 500 μL acetone and stainless steel beads (5 mm diameter) were added in each layer followed by homogenization for 10 min at 50 Hz using Tissue Lyser LT (Qiagen, Ltd., Manchester, UK) to extract CAR from the skin. Homogenized samples were then centrifuged at 14,800 rpm for 15 min and finally, a sample from supernatant was diluted with PBS (pH 7.4) before quantification of CAR using analytical method provided in Supplementary information S1. PK Solver software was used for data analysis by applying one-compartment open model and the kinetic parameters were calculated. Samples taken from receiving chamber were also analyzed using HPLC after making suitable dilutions with PBS (pH 7.4), and results were presented as drug permeated/unit area versus time. Eq. (5) was used to calculate flux:

$$J_{ss} = \left(\frac{dQ}{dt} \right)_{ss} * 1/A \quad (5)$$

where: J_{ss} = Steady state permeation flux (μg/cm²/h), A = Area of skin tissue, $(dQ/dt)_{ss}$ = Amount of CAR permeating through skin per unit time at a steady state (μg/h).

2.13. Determination of antibacterial effectiveness in an Ex-vivo pig skin wound model

The ability of CAR and CAR-PCL NPs loaded MN arrays to reduce bacterial colonization was determined in an *ex-vivo* neonatal porcine skin wound infection model using a previously reported method with slight modifications [43]. The skin samples were prepared following the same protocol mentioned in Section 2.9. The pig skin was cleansed with 70% ethanol and cut into equal circular patches of size 1.3 cm in diameter then was set into petri dishes having Kleenex paper (soaked in

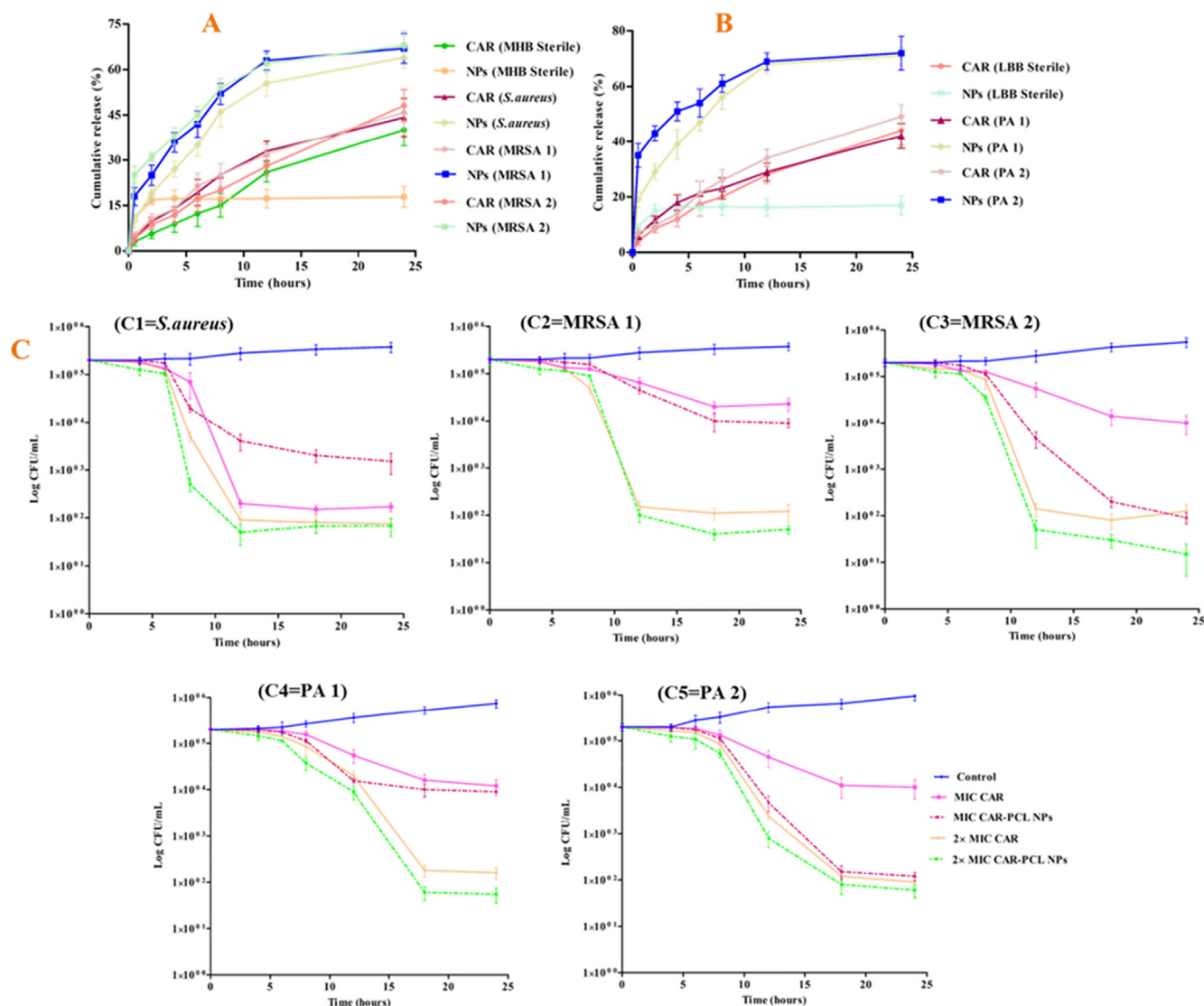


Fig. 1. (A) *In-vitro* release profiles of CAR and CAR-PCL NPs in the presence of lipase-secreting Gram-positive bacterial cultures (mean \pm SD, $n = 3$), including (*S. aureus* = *Staphylococcus aureus* (NCTC[®] 10788), (MRSA 1 = *Staphylococcus aureus* (ATCC[®] 33593TM), (MRSA 2 = *Staphylococcus aureus* [MW2] ATCC[®] BAA-1707TM), and sterile MHB without any bacteria. (B) *In-vitro* release profiles of CAR and CAR-PCL NPs in presence of lipase-secreting Gram-negative bacterial cultures (mean \pm SD, $n = 3$), including (PA 1 = *Pseudomonas aeruginosa* ATCC[®] 9027) and (PA 2 = *Pseudomonas aeruginosa* [PAO1] ATCC[®]BAA- 47) and sterile LBB without any bacteria. (C1–C5) Time kill assay of CAR and CAR-PCL NPs against *S. aureus*, MRSA 1, MRSA 2, PA 1 and PA 2 respectively.

sterile water) in the bottom. Red hot brass knob was used to make burn wounds of size 5 mm in diameter (circular) and 0.5 mm deep. Bacterial test strains were cultured and adjusted to a concentration of 2.0×10^5 CFU/mL in a similar way to the method in Section 2.4. 100 μ L of bacterial suspension was applied to all wounds. Petri dishes were covered with lids to establish a moist chamber, and then incubated at 37 $^{\circ}$ C for 4 h. Both the CAR-MNs and CAR-PCL NPs-MNs arrays were applied (for the same time as used in dermatokinetic studies) to the wounds and the petri dishes were incubated for 24 h at 37 $^{\circ}$ C. After 24 h treatment, each skin sample was placed into a 1.5 mL eppendorf tube, followed by addition of 1 mL of sterile PBS (pH 7.4), and homogenized utilizing Tissue Lyser LT (Qiagen, Ltd., Manchester, UK) at 50 Hz for 15 min to harvest bacteria from the skin. Finally, resultant bacterial suspensions were analysed for surviving CFUs by inoculating on MHA/LBA plates, followed by 48 h' incubation at 37 $^{\circ}$ C. Infected wounds without application of MN arrays were run as positive control and uninfected wounds were as a negative control. Experiments were performed in triplicate.

2.14. Statistical analysis

All tests/investigations were performed in triplicate and data were manifested as a mean \pm SD. Results were statistically analysed by unpaired *t*-test and ANOVA to determine statistical significance (specified at $p < 0.05$).

3. Results and discussion

3.1. Characterization of nanoparticles

In this study, NPs were prepared by employing a simple nanoprecipitation approach and characterized in terms of essential physico-chemical parameters, including particle size, PDI, ZP and EE. The particle size and PDI are essential parameters to determine width of size distribution and for subsequent drug permeation through skin. The CAR-PCL NPs have shown particle size of 198 nm with 0.04 PDI. Blank PCL NPs were found to be slightly lower in particle size (184 nm with 0.07 PDI) as compared to CAR-PCL NPs. Low value of PDI for both NPs

Table 1
MIC and MBC values of free CAR and CAR-PCL NPs.

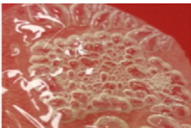
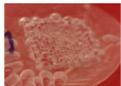
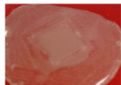
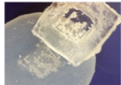
Bacterial strains	MIC (mg/mL)		MBC (mg/mL)	
	CAR	CAR-PCL NPs	CAR	CAR-PCL NPs
<i>Staphylococcus aureus</i> (NCTC® 10788)	0.156	0.078	0.156	0.156
<i>Staphylococcus aureus</i> (ATCC® 33593)	0.156	0.078	0.312	0.156
<i>Staphylococcus aureus</i> [MW2](ATCC® BAA-1707)	0.156	0.156	0.312	0.156
<i>Pseudomonas aeruginosa</i> [PAO1] (ATCC® BAA- 47)	0.625	0.312	1.25	0.312
<i>Pseudomonas aeruginosa</i> (ATCC® 9027)	0.312	0.156	0.625	0.312

have demonstrated the monodispersed and homogeneous nature of formulations. In order to optimize the concentration of cryoprotectant (PVP was used in this study) that can be used in lyophilization of CAR-PCL NPs, the effect of various concentrations of PVP (0.5–2% w/v) on

particle size after lyophilization was also investigated. It was observed that, at higher concentrations (1–2% w/v) of PVP, particle size was reduced after lyophilization, but NPs were found to be sticky in nature. However, at lower concentration (0.5% w/v), particle size remained unchanged and NPs were freely flowing. Therefore, 0.5% w/v PVP was used as a cryoprotectant in further experiments.

ZP is a key factor to evaluate the stability of colloidal dispersions [44]. It was found that the ZP of CAR- PCL NPs (-17.7 ± 7.21 mV) was increased, in comparison to blank PCL NPs (-13.7 ± 5.96 mV), indicating that CAR induced a more negative charge to the particles. This is in line with previously reported studies [45]. Moreover, negative surface charge is favorable for deeper skin penetration of NPs, as reported in previous studies [46]. Drug content entrapped in NPs is the most essential parameter in order to achieve desired therapeutic activity. CAR-PCL NPs exhibited $83.28 \pm 3.62\%$ EE, which is in agreement with previous studies, reporting greater than 80% encapsulation of hydrophobic drugs in PCL NPs using this method of NPs formulation [47,48]. Additionally, NR-PCL NPs were formulated and showed approximately same particle size (191 nm with 0.098 PDI) as that of CAR-

Table 2
Composition of formulations and casting methods used to fabricate CAR-PCL NPs loaded bilayer dissolving MN arrays.

Form. code	Composition (%w/w) *PVP (29–32 K), PVA (31–50 K)	Casting methods to produce CAR-PCL NPs loaded dissolving MN arrays	Representative images of the formed MN arrays		Observations and comments
F1	First layer: 25 NPs, 7.5 PVA, 10 PVP; Second layer: hydrogel of 15 PVA, 20 PVP	Two step casting was performed using pressure chamber method			All the needles were destroyed because of air bubbles
F2	First layer: 25 NPs, 7.5 PVA, 10 PVP; Second layer: hydrogel of 15 PVA, 20 PVP	Second layer was casted under vacuum after 24 h drying of first layer			Too many air bubbles appeared on surfaces which were removed with needle. In trying to remove bubbles, most of the gel was wasted resulting in too brittle/fragile base plate
F3	First layer: 30 NPs, 7.5 PVA, 10 PVP; Second layer: hydrogel of 15 PVA, 20 PVP	NPs hydrogel mix was poured into the molds with spatula instead of using syringe. Second layer was casted under vacuum			No air bubbles were found and MNs were intact. But NPs were diffused back in the base plate
F4	First layer: 30 NPs, 7.5 PVA, 10 PVP; Second layer: preformed base plate of 15 PVA, 20 PVP	MN arrays were casted in one step. NPs hydrogel mix was poured into the molds and preformed base plate was placed on it, followed by positive pressure. Metal weight was applied during 48 h drying period			Needles were remained in the molds upon demolding
F5	First layer: 30 NPs, 7.5 PVA, 10 PVP; Second layer: preformed base plate of 15 PVA, 20 PVP	First layer was casted following the same protocol as mentioned in text but in second step, preformed base plate was placed on needles with adding one drop of hydrogel followed by positive pressure. Metal weight was applied during 48 h drying			Very few needles were attached to the base plate and remaining was in the mold upon demolding
F6	First layer: 30 NPs, 7.5 PVA, 10 PVP; Second layer: preformed base plate of 15 PVA, 20 PVP	MN arrays were casted in the same way as F5 but without application of weight			Needles were not fully formed
F7	First layer: 30 NPs, 7.5 PVA, 10 PVP; Second layer: preformed base plate of 15 PVA, 20 PVP	One step casting (as F4) but no additional hydrogel or weight was applied			Not all the needles were attached to the base plate. Few needles were filled with NPs and remaining was with hydrogel
F8	First layer: 70 NPs, 30 water; Second layer: hydrogel of 20 PVA, 25 PVP	Casted in the same way as mentioned in Section 2.7			MN arrays were not of good mechanical strength
F9	First layer: 50 NPs, 6 PVA, 7.5 PVP; Second layer: hydrogel of 20 PVA, 25 PVP	Casted in the same way as mentioned in Section 2.7			MN arrays were intact upon removal from molds but broke off on applying 32 N force with texture analyzer
F10	First layer: 40 NPs, 8 PVA, 10 PVP; Second layer: hydrogel of 20 PVA, 25 PVP	Casted in the same way as mentioned in Section 2.7			Needles were sharp and fully formed with strong base plate

PCL NPs.

3.2. In-vitro release study of CAR-PCL NPs in bacterial cultures

Drug release studies provide information on the duration of drug availability. It was hypothesized that entrapment of CAR in PCL would inhibit its undesired leakage, but preferably in the presence of lipase-secreting bacteria, PCL would degrade to provide CAR to kill the bacteria. In order to evaluate the potential of on-demand delivery of PCL NPs, release studies were performed in both the absence and presence of lipase-secreting bacteria [Fig. 1(A and B)]. For the purpose, various strains of Gram-positive and negative bacteria known to release lipase enzyme were investigated (lipase-secreting activity of all the strains was confirmed using a Tween® 80 substrate based precipitation test; data not shown). Additionally, release pattern of CAR in the pure form was also determined in the presence and absence of all the test strains. CAR has not shown any significant difference ($p = 0.886$) in release profiles at all the test conditions. As depicted in Fig. 1(A and B), NPs showed a burst release in the first 30 min and, thereafter, a slow release of up to 67–72% in 24 h was obtained in all the bacterial cultures. In contrast, CAR in the pure form has shown significantly less ($p = 0.0378$) release (40–49% in 24 h) than NPs; this less release could be ascribed to the hydrophobic nature of the CAR. Initially, *Pseudomonas aeruginosa* [PAO1] showed greater release in comparison to other test strains, but there was no significant difference found ($p = 0.728$) in total drug release from NPs in all the bacterial cultures. In comparison to this, NPs in sterile broth media, showed significantly less release ($p = 0.003$) of 17% total in 24 h. Thus, the higher release of CAR from PCL NPs in the bacterial system, in contrast to sterile media, could be attributed to the presence of enzymes released by bacteria. These findings are also in line with the findings of Wu et al. [49], who reported that presence of enzyme increases the degradation rate of PCL by 1000 fold, in comparison to degradation in aqueous medium alone. A remarkable difference between the release of CAR in the presence and absence of bacteria demonstrated the suitability of the designed system for potential selective delivery at infection sites. Hence, these results have proven the concept that loading of CAR into a responsive NPs system can avoid its release at non-specific sites. All formulations exhibited maximum linearity for Korsmeyer–Peppas model (Table S3). Furthermore, n values (diffusion coefficient) for all NPs formulations were less than 0.4, suggesting simple Fickian diffusion of CAR from polymer [50].

3.3. Antimicrobial assays

3.3.1. Determination of minimum inhibitory concentration and minimum bactericidal concentration

The blank PCL NPs have not shown any antibacterial activity against test strains. Table 1 presents the MIC and MBC values of free CAR and CAR-PCL NPs against *S. aureus* and *Pseudomonas aeruginosa* strains. The results indicated that both free CAR and CAR-PCL NPs were more effective against Gram-positive strains than Gram-negative bacteria. The ratio of MBC to MIC was found to be < 4 in all cases, suggesting the bactericidal nature of both CAR and CAR-PCL NPs; as an antimicrobial is considered to be bactericidal if ratio of MBC to MIC is ≤ 4 and bacteriostatic if it is > 4 [51]. Importantly, MIC and MBC values for CAR-PCL NPs were lower than free CAR indicating that loading of CAR in NPs has improved its antibacterial activity. Kamimura et al. [52], obtained similar results, showing that micro-encapsulation of CAR in hydroxypropyl-beta-cyclodextrin, significantly improved its antibacterial potential. Enhanced antibacterial activity of NPs might be due to several reasons; however, as the primary site for antimicrobial action of CAR is at the membrane and inside cytoplasm of pathogen, the NPs may have increased CAR access to these regions by increasing its solubility. Thus, these results highlight the potential of the developed CAR-PCL NPs to be used for enhanced antibacterial

activity, in addition to site-specific delivery.

3.3.2. Time kill assay

Time kill curves of free CAR and CAR-PCL NPs against lipase-secreting bacteria are displayed in [Fig. 1(C1–C5)]. As illustrated in the figure, both CAR and CAR-PCL NPs showed significant inhibition of viable bacterial count for all test strains in comparison to their untreated controls. In all the cases, both the CAR and CAR-PCL NPs have shown rapid bacterial inhibition at higher concentrations ($2 \times \text{MIC}$) in comparison to lower concentrations (MIC), suggesting concentration dependent killing kinetics. Moreover, at all MICs, CAR-PCL NPs have shown greater and faster reduction of bacterial growth in contrast to free CAR. This rapid killing is as important as the bactericidal nature of the compound, because the quicker the antimicrobial agent kills, the more efficiently it can block biofilm formation [53].

3.4. Fabrication of dissolving MN arrays

The composition of various polymers blends used to fabricate CAR-PCL NPs loaded MN arrays is given in Table 2 along with casting methods. As illustrated by the representative images of the formulated MN arrays (provided in Table 2), CAR-PCL NPs formulation was not suitable to fabricate MN arrays using compression in a pressure chamber (F1–F7). In contrast, the centrifugation approach was found to be successful in concentrating NPs in the tips of needles, avoiding their diffusion back in to the baseplate. After optimization of steps of casting method, NPs were mixed with PVA/PVP hydrogel in different concentrations (F8–F10); in order to find an optimum ratio that can result in maximum loading of NPs in needles and desired mechanical strength. F10 was found to be the most promising formulation which resulted in fully formed and strong MN arrays. Digital images obtained using Leica EZ4D digital microscope and SEM images of optimized MN arrays are provided in Fig. 2.

Fabrication of bilayer MN arrays having NPs concentrated in their tips (CAR-PCL NPs-MNs) could favor the rapid administration of CAR loaded PCL cargos into the viable layers of the skin, upon the dissolution of a supportive PVA/PVP matrix. Moreover, this approach could be beneficial for drug delivery without wastage of drug and with short application time. In order to confirm that NPs are concentrated in the needle tips; NR-PCL NPs loaded MN arrays were fabricated following the same protocol and formulation composition as for optimized CAR-PCL NPs loaded bilayer MN arrays, to facilitate the imaging. Microscopic images of NR-PCL NPs loaded MN arrays [Fig. 2(c1,c2)] clearly showed that NPs are concentrated in the needle tips.

3.5. Evaluation of mechanical strength and insertion properties of MN arrays

The selected formulations of dissolving MN arrays were subjected to a compression test in order to investigate their mechanical strength. Both the formulations showed reduction in needles height (notably without being fractured, rather being compressed slightly) upon application of 32 N force/array, as displayed in Fig. 3(b). The percentage reduction in the MN height for CAR-MNs and CAR-PCL NPs-MNs was calculated to be 8.73% and 10.46%, respectively, suggesting no significant difference in both formulations ($p = 0.98$). In order to estimate the penetration depth of MNs in the skin, eight layers of Parafilm M® were used. Both the MN arrays showed 100% penetration in the first layer, 87–91% in the second layer and $> 25\%$ in the third layer. Digital images of the microconduits created in Parafilm M® layers are provided in Fig. 3(a: 1–3). Additionally, to visualize the insertion of MN arrays in the layers of laboratory film, OCT images were recorded, which further confirmed the penetration of MNs up to the third layer as illustrated in the Fig. 3(d: 1–2). As reported by Larrañeta et al. [39], penetration is considered successful if $> 20\%$ microconduits are created in each layer, thus, it can be considered that MNs are lying in between the third

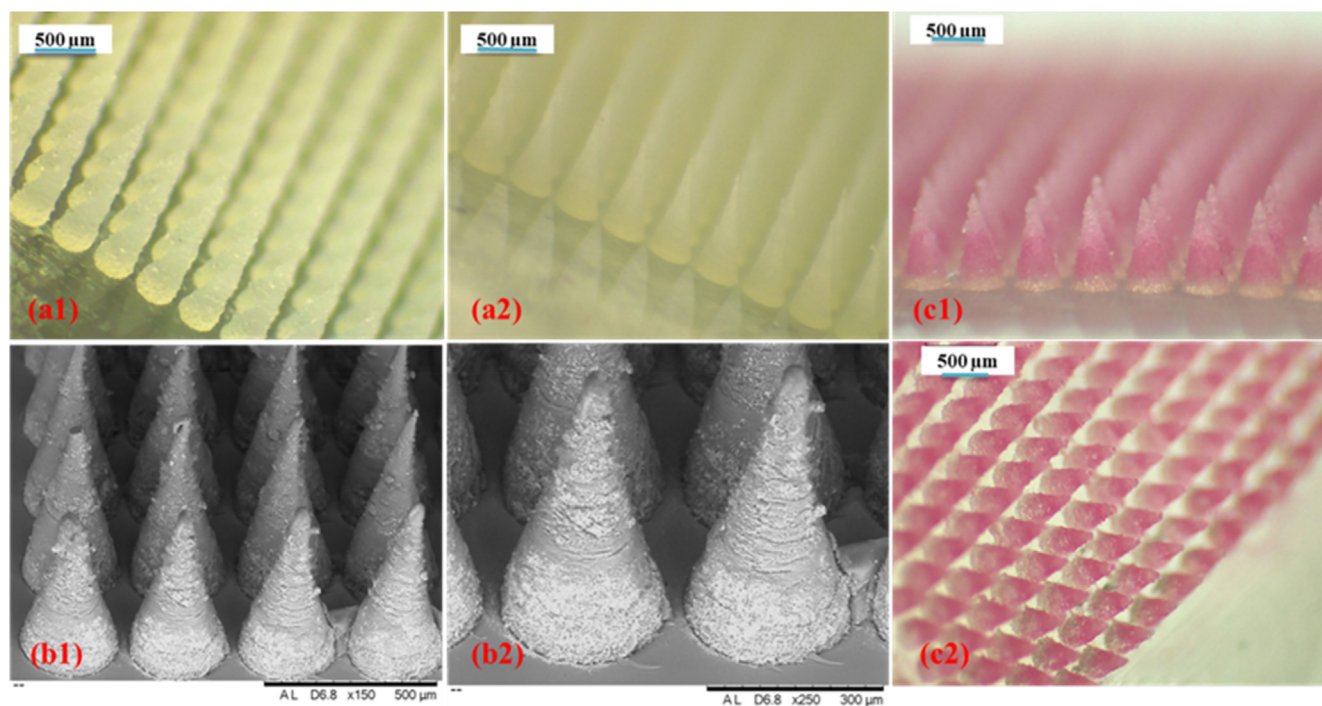


Fig. 2. Digital pictures of dissolving MN arrays (19×19) taken with Leica EZ4D digital microscope; (a1, a2) CAR and CAR-PCL NPs-MN arrays, and (c1, c2) NR-PCL NPs-MN arrays, (b1, b2) SEM images of CAR and CAR-PCL NPs-MN arrays. To use as a control in dermatokinetic studies, free CAR loaded MN arrays were also fabricated using the same molds (19×19 , conical) as for NPs loaded MN arrays. Various FDA approved commonly used pharmaceutical polymers were tested for their potential to be used as matrices in the formation of dissolving MN arrays loaded with a high content of CAR. Representative images along with brief comments about identified properties of all the formulations tested are provided in Table S2. The final formulation [2%w/w carvacrol: 1% w/w Tween® 80: 16% w/w PVA (31–50 K): 20% w/w PVP (29–32 K)] was found promising for the fabrication of fully formed needles with required mechanical strength. Images taken with digital microscope and SEM are given in (a, b).

and fourth layers. Moreover, the thickness of one Parafilm M® layer is approximately $126 \pm 7 \mu\text{m}$, suggesting that MNs were penetrated up to $378 \mu\text{m}$ depth (approximately 63% of needles height). These findings are in line with previously published work reporting 60% insertion of the total needle height using the same design [39]. Hence, these results indicated that the MN arrays fabricated here are mechanically strong enough, which could help in penetration across necrotic/hyperkeratotic tissue barrier.

3.6. In-skin dissolution of MN arrays

The dissolution kinetics of the developed MN arrays was investigated in the neonatal porcine skin and representative images are given in Fig. S1. As depicted in the figure, dissolution of both the MN arrays was very fast; showing dissolution in 9 min after insertion into the skin. However, CAR-MNs had shown slightly faster dissolution than CAR-PCL NPs-MNs, as these were completely disappeared in first 5 min of application. The delivery of NPs in the skin depends upon the dissolution of polymeric matrices of the needles in the interstitial fluid of the skin. The fast dissolution of the MNs, suggests rapid delivery of NPs into the skin layers.

3.7. Calculation of drug content in MN arrays

Upon drying and subsequent removal of side walls, average CAR content in CAR-MNs was found to be $5.74 \pm 1.05 \text{ mg/array}$ (Mean \pm SD, $n = 5$), out of which only $205 \mu\text{g} \pm 17 \mu\text{g}$ was located in the needles. Similar concentrations of CAR were found to be located in the needles of CAR-PCL NPs-MNs i.e. $195 \mu\text{g} \pm 13 \mu\text{g}$.

3.8. Particle size determination after loading into MN arrays

The average particle size was not changed significantly ($218 \pm 9 \text{ nm}$) after formulation of MN arrays. This can be explained as the polymer matrix of MNs might work as a stabilizer for CAR-PCL NPs particle size

3.9. Ex-vivo dermatokinetic studies

The results demonstrated that the concentration of CAR in dermal layers was considerably higher ($p < 0.05$) using CAR-PCL NPs-MNs as compared to CAR-MNs. Fig. 4 describes the comparison of kinetic profile of CAR (concentration versus time) in both epidermis (a) and dermis (b) layers of porcine skin followed by the application of CAR-PCL NPs-MNs in comparison with CAR-MNs. The dermatokinetic profile of CAR-MNs depicted that the C_{max} in the epidermis was found to be $73.22 \pm 5.48 \mu\text{g}/\text{cm}^3$ after $1.42 \pm 0.46 \text{ h}$. In the dermis, the highest concentration of $116.61 \pm 14.61 \mu\text{g}/\text{cm}^3$ was achieved in $1.59 \pm 0.39 \text{ h}$. The AUC_{0–24} of CAR in the epidermis was $861.44 \pm 32.64 \text{ h} \cdot \mu\text{g}/\text{cm}^3$ and in the dermis was found to be $1384.23 \pm 167.37 \text{ h} \cdot \mu\text{g}/\text{cm}^3$. With respect to the profile of CAR-PCL NPs-MNs in the epidermis, the t_{max} was found to be $1.45 \pm 0.67 \text{ h}$ with a concentration of $59.15 \pm 10.39 \mu\text{g}/\text{cm}^3$. In the dermis, C_{max} ($110.67 \pm 19.76 \mu\text{g}/\text{cm}^3$) was achieved in $1.77 \pm 0.71 \text{ h}$. The AUC_{0–24} in the epidermis was $1252.95 \pm 187.16 \text{ h} \cdot \mu\text{g}/\text{cm}^3$ and in the dermis was determined to be $2457.61 \pm 243.08 \text{ h} \cdot \mu\text{g}/\text{cm}^3$. All dermatokinetic parameters for both the MN arrays are provided in supplementary Table S4.

The values of AUC_{0–24} of CAR-PCL NPs-MNs in both the epidermis and dermis were found to be considerably higher ($p < 0.05$ each) than those of CAR-MNs suggesting enhanced retention of CAR in skin layers after incorporation into NPs. The results of the permeation study further

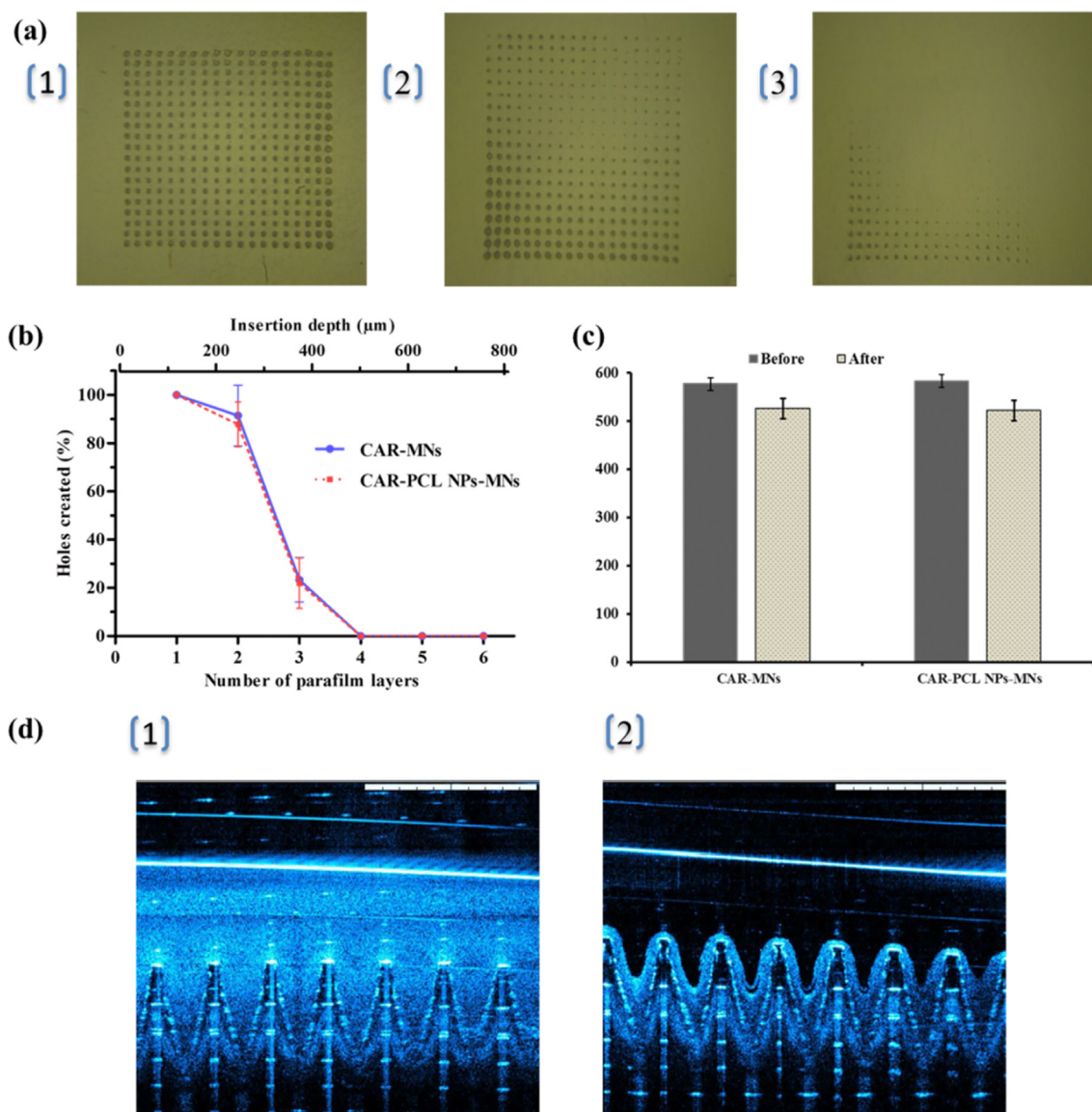


Fig. 3. (a) Images of the first three layers of Parafilm M® presenting microconduits in each layer created upon insertion of MN arrays, (b) percentage of holes created in each Parafilm M® layer for estimation of MN insertion depth, (c) Compression analysis of CAR-MNs and CAR-PCL NPs-MNs. Before compression, needle height for CAR-MNs was $577 \pm 17.32 \mu\text{m}$, and for CAR-PCL NPs-MNs was $583 \pm 14.19 \mu\text{m}$ (means \pm SD, $n = 5$) which was reduced to $526 \pm 16.47 \mu\text{m}$ and $522 \pm 15.13 \mu\text{m}$ respectively upon application of 32 N force/array, (d) Representative OCT images illustrating insertion of MN arrays in Parafilm M® layers; (1) CAR-MNs and (2) CAR-PCL NPs-MNs. False colors were applied to the MN arrays. A white scales bar at top right corner is representing a length of 1 mm.

supported the retention potential of CAR-PCL NPs in skin layers. As demonstrated in Fig. 4(c), free CAR has shown significantly higher permeation ($p < 0.05$) as compared to CAR-PCL NPs. A percentage comparison between CAR and CAR-PCL NPs MNs in terms of CAR retention in skin layers and permeation at different time points is presented in Fig. 4(d). As displayed in the figure (d), in case of both CAR-MNs and CAR-PCL NPs-MNs, approximately 90% of the total applied CAR (content loaded into the needles) was successfully delivered. Considering the total amount of CAR delivered through MN arrays, a significant percentage of CAR was found in the skin layers for CAR-PCL NPs-MNs ($26.04 \pm 3.45\%$ in epidermis and $55.43 \pm 5.28\%$ in dermis) even after 24 h of application, in contrast to CAR-MNs showing very negligible percentages in the epidermis ($2.01 \pm 0.09\%$) and the dermis ($5.29 \pm 1.95\%$).

With respect to the required concentration of CAR for antimicrobial activity, as described in Section 3.3.2, 0.156 mg/mL to 0.312 mg/mL of CAR-PCL NPs can kill $> 99.9\%$ bacteria within 12–18 h. The concentration of CAR-PCL NPs achieved with CAR-PCL NPs-MNs in the

dermatokinetic study was above 0.156 mg/mL and remained available at desired site for more than 24 h demonstrating the suitability of CAR-PCL NPs for site-specific delivery of CAR. In contrast, free CAR was required in higher concentrations (0.156–1.25 mg/mL) to show the same inhibitory effect, while the concentration of CAR obtained in dermatokinetic study was much lower than its required effective concentration. Moreover, its residence time was also very short, not sufficient for CAR to show its desired antimicrobial activity. Hence, these results have proven the concept of this study that loading of CAR into NPs could be an effective approach to enhance its availability at site of action with improved antimicrobial activity. Furthermore, to deliver the required concentrations, increased loading of NPs into the needles could be considered. This would be advantageous in terms of short application time as these fast dissolving bilayer MNs can administer NPs rapidly into the skin, which subsequently can act as drug depots to release the CAR in response to bacterial infection.

Loading of CAR in NPs and then further into MN arrays has significantly improved its sustained delivery into the dermal layers and,

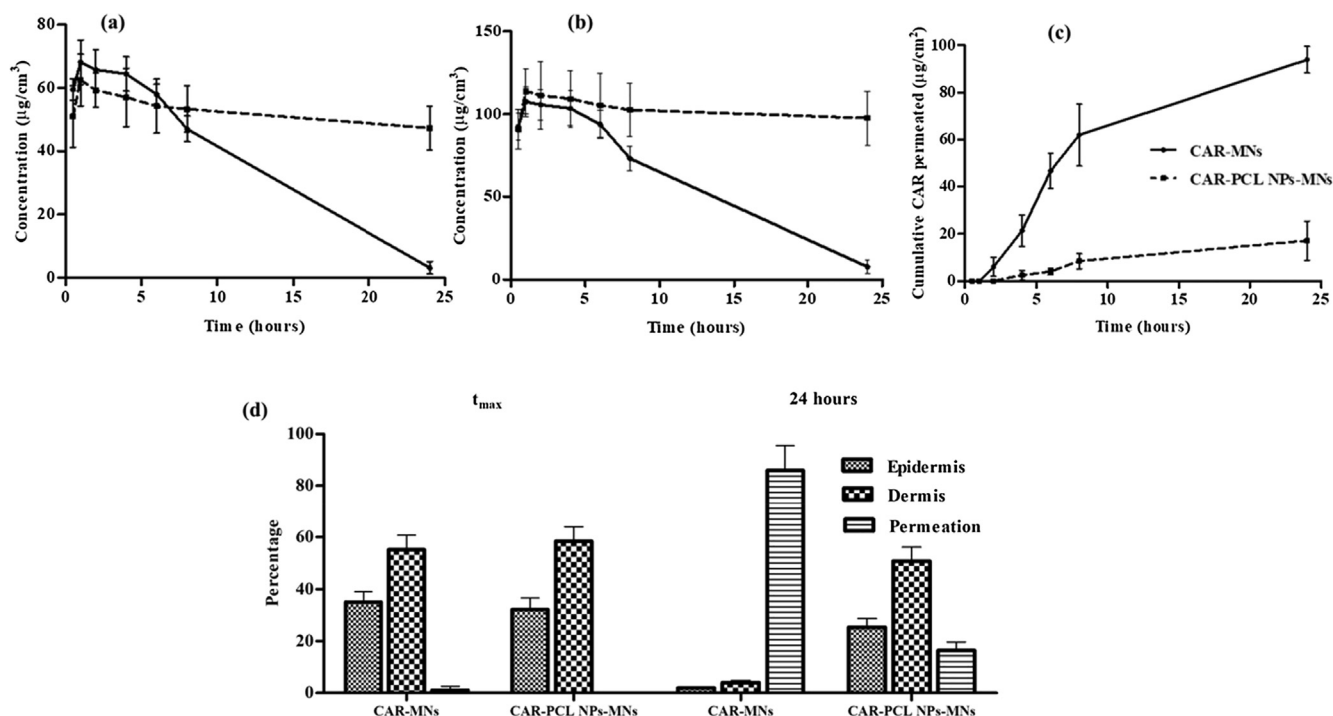


Fig. 4. (a) CAR concentration and time profile in epidermis and (b) Dermis and (c) Cumulative CAR permeation through excised full-thickness neonatal porcine skin followed by the application of CAR-PCL NPs-MNs in comparison with CAR-MNs (means \pm S.D., $n = 3$), (d) Comparison of CAR percentage permeated and CAR percentage retention in the epidermis and dermis layers (considering the total amount applied) of the skin at t_{max} and 24 h following the application of CAR-PCL NPs-MN arrays in comparison with CAR-MNs (means \pm S.D., $n = 3$).

hence, could potentially be used for management of a variety of chronic wound infections. However, further *in-vivo* studies must be conducted to investigate the kinetic profiles of CAR in wound infection models.

3.10. Determination of antibacterial effectiveness in an *ex-vivo* pig skin wound model

Post infection CFU counts in an *ex-vivo* neonatal porcine skin wound infection model demonstrated a significant reduction in microbial burden in treated groups in comparison to untreated ones. The reduction in microbial burden was higher in the case of Gram-positive bacteria in comparison to Gram-negative bacteria, as also indicated by higher MIC/MBC values of CAR and NPs against Gram-negative strains. The CAR-MNs showed $99.9 \pm 0.09\%$ reduction in microbial burden in wounds infected by NCTC® 10788, $90.12 \pm 3.21\%$ reduction in ATCC®33593™ and $94.12 \pm 3.21\%$ reduction in ATCC® BAA-1707™. In contrast, CAR-PCL NPs-MNs showed approximately 98–99.9% inhibition of microbial load for all *S. aureus* strains. In case of *Pseudomonas aeruginosa* test strains, the CAR-MNs showed only $39.9 \pm 4.19\%$ reduction in ATCC® 9027 and $21 \pm 2.08\%$ reduction in ATCC®BAA- 47, while CAR-PCL NPs-MNs have shown $87 \pm 2.41\%$ reduction in ATCC® 9027 and $80 \pm 2.61\%$ reduction in ATCC®BAA-47. In this *ex-vivo* infection model, CAR-MNs have also shown $> 90\%$ inhibition against *S. aureus* test strains, because it was a closed system and the entire drug applied was retained at the application site (that probably will not happen in an *in-vivo* open model). In contrast, significantly less inhibition was achieved in case of Gram-negative strains because the concentrations available were lower than required therapeutic concentrations (less loading into the MNs). However, CAR-PCL NPs-MNs have shown considerable antimicrobial effect even against Gram-negative bacteria because of their antimicrobial potential at lower concentrations. The current results have proven the concept of the study that MNs can efficiently deliver the NPs into the skin and subsequently NPs can show their antimicrobial effect at the site of infection. However, it is required to investigate the antimicrobial

effectiveness of developed formulations in an animal model to estimate actual behavior of the formulations.

4. Conclusion

The current study demonstrated the potential of the designed CAR-PCL NPs to release the drug in response of bacterial infection and improved antimicrobial activity of CAR against both Gram-positive and Gram-negative bacteria. Furthermore, these designed NPs were successfully loaded into the dissolving MN arrays and the results of *in-vitro/ex-vivo* characterization of developed MN arrays have indicated their suitability in terms of dermal application and rapid delivery of NPs to the desired site. The overriding advantage of this developed site-specific delivery approach presented here, in comparison to application of pure compound, lies in the MNs capacity to deliver the NPs directly to the site of infection and further in NPs potential to be retained in the skin for longer duration which could potentially result in sustained desired antimicrobial effect avoiding multiple applications. The results have proven the concept of the study that the designed delivery platform can be used as a potential viable alternative treatment approach to that of conventional antibiotics and dosage forms for management of chronic wound infections. This proof of concept finding provided a starting point for a number of follow-up investigations including, biocompatibility studies, and pharmacokinetics and pharmacodynamics studies in suitable animal models. We are currently developing these investigations.

Acknowledgments

The authors are thankful to Higher Education Commission of Pakistan and Commonwealth Scholarship Commission, United Kingdom for providing Scholarships to support this study.

Funding

Maria Mir is a PHD student funded by Indigenous PHD Fellowship Program, Higher Education Commission, Pakistan and Split Site PHD Scholarship, Commonwealth Scholarship Commission, United Kingdom. This work was also supported, in part, by Wellcome Trust grant number WT094085MA.

Appendix A. Supplementary material

Supplementary data to this article can be found online at <https://doi.org/10.1016/j.ejpb.2019.12.008>.

References

- [1] R.S. Howell-Jones, M.J. Wilson, K.E. Hill, A.J. Howard, P.E. Price, D.W. Thomas, A review of the microbiology, antibiotic usage and resistance in chronic skin wounds, *J. Antimicrob. Chemother.* 55 (2005) 143–149, <https://doi.org/10.1093/jac/dkh513>.
- [2] L. Gould, P. Abadir, H. Brem, M. Carter, T. Conner-Kerr, J. Davidson, L. Dipietro, V. Falanga, C. Fife, S. Gardner, E. Grice, J. Harmon, W.R. Hazzard, K.P. High, P. Houghton, N. Jacobson, R.S. Kirsner, E.J. Kovacs, D. Margolis, F. McFarland Horne, M.J. Reed, D.H. Sullivan, S. Thom, M. Tomic-Canic, J. Walston, J. Whitney, J. Williams, S. Ziemann, K. Schmader, Chronic wound repair and healing in older adults: current status and future research, *Wound Repair Regen.* 23 (2015) 1–13, <https://doi.org/10.1111/wrr.12245>.
- [3] C.K. Sen, G.M. Gordillo, S. Roy, R. Kirsner, L. Lambert, T.K. Hunt, F. Gottrup, G.C. Gurtner, M.T. Longaker, Human skin wounds: a major and snowballing threat to public health and the economy, *Wound Repair Regen.* 17 (2009) 763–771, <https://doi.org/10.1111/j.1524-475X.2009.00543.x>.
- [4] M. Clinmicroreps, P. Bowler, D.G. Armstrong, Wound microbiology and associated approaches to wound, *Clin. Microbiol. Rev.* 14 (2016) 244–269, <https://doi.org/10.1128/CMR.14.2.244>.
- [5] G.V. Doern, R.N. Jones, M.A. Pfaller, K.C. Kugler, M.L. Beach, Bacterial pathogens isolated from patients with skin and soft tissue infections: Frequency of occurrence and antimicrobial susceptibility patterns from the SENTRY Antimicrobial Surveillance Program (United States and Canada), *Diagn. Microbiol. Infect. Dis.* 34 (1999) 65–72, [https://doi.org/10.1016/S0732-8893\(98\)00162-X](https://doi.org/10.1016/S0732-8893(98)00162-X).
- [6] G. Cabot, L. Zamorano, B. Moyà, C. Juan, A. Navas, J. Blázquez, A. Oliver, Evolution of *Pseudomonas aeruginosa* antimicrobial resistance and fitness under low and high mutation rates, *Antimicrob. Agents Chemother.* 60 (2016) 1767–1778, <https://doi.org/10.1128/AAC.02676-15.Address>.
- [7] D.C. Kaur, S.S. Chate, Study of antibiotic resistance pattern in methicillin resistant staphylococcus aureus with special reference to newer antibiotic, *J. Glob. Infect. Dis.* 7 (2015) 78–84, <https://doi.org/10.4103/0974-777X.157245>.
- [8] R.D. E.B. Arbeit, D. Maki, F.P. Tally, E. Campanaro, The safety and efficacy of daptomycin for the treatment of complicated skin and skin-structure infections, *Clin. Infect. Dis.* 38 (2004) 1673–1681, <https://doi.org/10.1097/01.idc.0000144912.27311.19>.
- [9] M.M. Traczewski, B.D. Katz, J.N. Steenbergen, S.D. Brown, Inhibitory and bactericidal activities of daptomycin, vancomycin, and teicoplanin against methicillin-resistant *Staphylococcus aureus* isolates collected from 1985 to 2007, *Antimicrob. Agents Chemother.* 53 (2009) 1735–1738, <https://doi.org/10.1128/AAC.01022-08>.
- [10] K.M. Krause, M. Renelli, S. Difuntorum, T.X. Wu, D.V. Debabov, B.M. Benton, In-vitro activity of telavancin against resistant gram-positive bacteria, *Antimicrob. Agents Chemother.* 52 (2008) 2647–2652, <https://doi.org/10.1128/AAC.01398-07>.
- [11] D.B. Gilmer, J.E. Schmitz, C.W. Euler, V.A. Fischetti, Novel bacteriophage lysin with broad lytic activity protects against mixed infection by streptococcus pyogenes and methicillin-resistant staphylococcus aureus, *Antimicrob. Agents Chemother.* 57 (2013) 2743–2750, <https://doi.org/10.1128/AAC.02526-12>.
- [12] S. Prabuseenivasan, M. Jayakumar, S. Ignacimuthu, In-vitro antibacterial activity of some plant essential oils, *BMC Complem. Altern. Med.* 6 (2006) 1–8, <https://doi.org/10.1186/1472-6882-6-39>.
- [13] A. La Stora, D. Ercolini, F. Marinello, R. Di Pasqua, F. Villani, G. Mauriello, Atomic force microscopy analysis shows surface structure changes in carvacrol-treated bacterial cells, *Res. Microbiol.* 162 (2011) 164–172, <https://doi.org/10.1016/j.resmic.2010.11.006>.
- [14] Antonia Nostro, Teresa Papalia, Antimicrobial activity of carvacrol: current progress and future perspectives, *Recent Pat. Antiinfect. Drug Discov.* 7 (2012) 28–35, <https://doi.org/10.2174/157489112799829684>.
- [15] A. Marchese, C.R. Arciola, E. Coppo, R. Barbieri, D. Barreca, S. Chebaibi, E. Sobarzo-Sánchez, S.F. Nabavi, S.M. Nabavi, M. Daglia, The natural plant compound carvacrol as an antimicrobial and anti-biofilm agent: mechanisms, synergies and bio-inspired anti-infective materials, *Biofouling* 34 (2018) 630–656, <https://doi.org/10.1080/08927014.2018.1480756>.
- [16] A. Mouwakheh, A. Kincses, M. Nové, T. Mosolygó, C. Mohácsi-Farkas, G. Kiskó, G. Spengler, Nigella sativa essential oil and its bioactive compounds as resistance modifiers against *Staphylococcus aureus*, *Phyther. Res.* 33 (2019) 1010–1018, <https://doi.org/10.1002/ptr.6294>.
- [17] M.Y. Gunal, A.O. Heper, N. Zaloglu, The effects of topical carvacrol application on wound healing process in male rats, *Pharmacogn. J.* 6 (2014) 10–14, <https://doi.org/10.5530/pj.2014.3.2>.
- [18] Roberto Scaffaro, Francesco Lopresti, Manuela D'Arrigo, Andreama Marino, Antonia Nostro, Efficacy of poly(lactic acid)/carvacrol electropore membranes against *Staphylococcus aureus* and *Candida albicans* in single and mixed cultures, *Appl. Microbiol. Biotechnol.* 102 (9) (2018) 4171–4181 <http://link.springer.com/10.1007/s00253-018-8879-7https://doi.org/10.1007/s00253-018-8879-7>.
- [19] A. Nostro, R. Scaffaro, L. Botta, A. Filocamo, A. Marino, G. Bisignano, Effect of temperature on the release of carvacrol and cinnamaldehyde incorporated into polymeric systems to control growth and biofilms of *Escherichia coli* and *Staphylococcus aureus*, *Biofouling* 31 (2015) 639–649, <https://doi.org/10.1080/08927014.2015.1079703>.
- [20] P. Huiras, D. Pharm, J.K. Logan, D. Pharm, S. Papadopoulos, D. Pharm, D. Whitney, D. Pharm, Local antimicrobial administration for prophylaxis of surgical site infections, *Pharmacotherapy.* 32 (2012) 1006–1019, <https://doi.org/10.1002/phar.1135>.
- [21] R.S. Kalhapure, M. Jadhav, S. Rambharose, C. Mocktar, S. Singh, J. Renukuntla, T. Govender, pH-responsive chitosan nanoparticles from a novel twin-chain anionic amphiphile for controlled and targeted delivery of vancomycin, *Colloids Surf. B Biointerf.* 158 (2017) 650–657, <https://doi.org/10.1016/j.colsurfb.2017.07.049>.
- [22] H. Hathaway, J. Ajuebor, L. Stephens, A. Coffey, U. Potter, J.M. Sutton, A.T.A. Jenkins, Thermally triggered release of the bacteriophage endolysin CHAPK and the bacteriocin lysostaphin for the control of methicillin resistant *Staphylococcus aureus* (MRSA), *J. Control. Release.* 245 (2017) 108–115, <https://doi.org/10.1016/j.jconrel.2016.11.030>.
- [23] D.G. Meecker, S.V. Jenkins, E.K. Miller, K.E. Beenken, A.J. Loughran, A. Powless, T.J. Muldoon, E.I. Galanzha, V.P. Zharov, M.S. Smeltzer, J. Chen, Synergistic photothermal and antibiotic killing of biofilm-associated *Staphylococcus aureus* using targeted antibiotic-loaded gold nanoconstructs, *ACS Infect. Dis.* 2 (2016) 241–250, <https://doi.org/10.1021/acscinfed.5b00117>.
- [24] Y. Zhang, J. Zhang, W. Chen, P. Angsantikul, K.A. Spiekermann, R.H. Fang, W. Gao, L. Zhang, Erythrocyte membrane-coated nanogel for combinatorial antivirulence and responsive antimicrobial delivery against *Staphylococcus aureus* infection, *J. Control. Release.* 263 (2017) 185–191, <https://doi.org/10.1016/j.jconrel.2017.01.016>.
- [25] Y. Suzuki, M. Tanihara, Y. Nishimura, K. Suzuki, Y. Kakimaru, Y. Shimizu, A new drug delivery system with controlled release of antibiotic only in the presence of infection, *J. Biomed. Mater. Res.* 42 (1998) 112–116, [https://doi.org/10.1002/\(SICI\)1097-4636\(199810\)42:1<112::AID-JBM14>3.0.CO;2-N](https://doi.org/10.1002/(SICI)1097-4636(199810)42:1<112::AID-JBM14>3.0.CO;2-N).
- [26] Y. Li, G. Liu, X. Wang, J. Hu, S. Liu, Enzyme-responsive polymeric vesicles for bacterial-strain-selective delivery of antimicrobial agents, *Angew. Chem. Int. Ed.* 55 (2016) 1760–1764, <https://doi.org/10.1002/anie.201509401>.
- [27] M. Xiong, Y. Bao, X. Yang, Y. Wang, B. Sun, J. Wang, Lipase-sensitive polymeric triple-layered nanogel for “On-Demand” drug delivery, *J. Am. Chem. Soc.* 134 (2012) 4355–4362, <https://doi.org/10.1021/ja211279u>.
- [28] S.P.N. Ms, H.S. Courtney, J.D. Bumgardner, W.O. Haggard, Chitosan sponges to locally deliver amikacin and vancomycin A pilot in vitro evaluation, *Clin. Orthop. Relat. Res.* 468 (2010) 2074–2080, <https://doi.org/10.1007/s11999-010-1324-6>.
- [29] J.S. Boateng, K.H. Matthews, H.N.E. Stevens, G.M. Eccleston, Wound healing dressings and drug delivery systems: a review, *J. Pharm. Sci.* 97 (2008) 2892–2923, <https://doi.org/10.1002/jps.21210>.
- [30] B.A. Lipsky, C. Hoey, Topical antimicrobial therapy for treating chronic wounds, *Clin. Infect. Dis.* 49 (2009) 1541–1549, <https://doi.org/10.1086/644732>.
- [31] T.S. Stashak, D. Acvs, E. Farstvedt, A. Othic, Update on wound dressings : indications and best use, *Clin. Tech. Equine Pract.* 3 (2004) 148–163, <https://doi.org/10.1053/j.ctep.2004.08.006>.
- [32] D.C. Roy, S. Tomblin, K.M. Isaac, C.J. Kowalczewski, D.M. Burmeister, L.R. Burnett, R.J. Christy, Ciprofloxacin-loaded keratin hydrogels reduce infection and support healing in a porcine partial-thickness thermal burn, *Wound Repair Regen.* 24 (2016) 657–668, <https://doi.org/10.1111/wrr.12449>.
- [33] E. Caffarel-salvador, M. Kearney, R. Mairs, L. Gallo, S.A. Stewart, A.J. Brady, R.F. Donnelly, Methylene blue-loaded dissolving microneedles: potential use in photodynamic antimicrobial chemotherapy of infected wounds, *Pharmaceutics* 7 (2015) 397–412, <https://doi.org/10.3390/pharmaceutics7040397>.
- [34] R. Raj, T. Singh, I. Tekko, K. Mcavoy, R.F. Donnelly, H. Mcmillian, D. Jones, Minimally invasive microneedles for ocular drug delivery, *Exp. Opin. Drug Deliv.* 5247 (2016) 525–537, <https://doi.org/10.1080/17425247.2016.1218460>.
- [35] M. Zaric, O. Lyubomska, O. Touzelet, C. Poux, S. Al-zahrani, F. Fay, L. Wallace, D. Terhorst, B. Malissen, S. Henri, U.F. Power, C.J. Scott, R.F. Donnelly, A. Kissenpfennig, Skin dendritic cell targeting via microneedle arrays laden with co-glycolide nanoparticles induces efficient antitumor and antiviral, *ACS Nano* 7 (2013) 2042–2055, <https://doi.org/10.1021/nn304235j>.
- [36] M. Radaeli, B. Parraga, L. Weidlich, L. Hoehne, A. Flach, L.A. Mendonc, E. Miranda, Antimicrobial activities of six essential oils commonly used as condiments in Brazil against *Clostridium perfringens*, *Brazil. J. Microbiol.* 47 (2016) 424–430, <https://doi.org/10.1016/j.bjm.2015.10.001>.
- [37] I. Khan, A. Bahuguna, P. Kumar, V.K. Bajpai, Antimicrobial potential of carvacrol against uropathogenic *Escherichia coli* via membrane disruption, depolarization, and reactive oxygen species generation, *Front. Microbiol.* 8 (2017) 1–9, <https://doi.org/10.3389/fmicb.2017.02421>.
- [38] R.F. Donnelly, R. Majithiya, T. Raghu, R. Singh, D.L.J. Morrow, M.J. Garland, Y.K. Demir, E. Ryan, D. Gillen, C.J. Scott, A.D. Woolfson, Design, optimization and characterisation of polymeric microneedle arrays prepared by a novel laser-based micromoulding technique, *Pharm. Res.* 28 (2011) 41–57, <https://doi.org/10.1007/s11095-010-0169-8>.

- [39] E. Larrañeta, J. Moore, E.M. Vicente-pérez, P. González-vázquez, R. Lutton, A.D. Woolfson, R.F. Donnelly, A proposed model membrane and test method for microneedle insertion studies, *Int. J. Pharm.* 472 (2014) 65–73, <https://doi.org/10.1016/j.ijpharm.2014.05.042>.
- [40] A. Summerfield, M.E. Ricklin, The immunology of the porcine skin and its value as a model for human skin, *Mol. Immunol.* 66 (2015) 14–21, <https://doi.org/10.1016/j.molimm.2014.10.023>.
- [41] M.T.C. Mc, E. Larrañeta, A. Clark, C. Jarrahan, A. Rein-weston, S. Lachau-durand, N. Niemeijer, P. Williams, C. Haec, H.O. Mccarthy, D. Zehrun, R.F. Donnelly, Design, formulation and evaluation of novel dissolving microarray patches containing a long-acting rilpivirine nanosuspension, *J. Control. Release.* 292 (2018) 119–129, <https://doi.org/10.1016/j.jconrel.2018.11.002>.
- [42] A.D. Permana, T.C. Mccrudden, R.F. Donnelly, Enhanced intradermal delivery of nanosuspensions of antifilaria drugs using dissolving microneedles: a proof of concept study, *Pharmaceutics* 11 (2019) 1–22, <https://doi.org/10.3390/pharmaceutics11070346>.
- [43] E. Myhrman, J. Håkansson, K. Lindgren, C. Björn, V. Sjöstrand, The novel antimicrobial peptide PXL150 in the local treatment of skin and soft tissue infections, *Appl. Microbiol. Biotechnol.* 97 (2013) 3085–3096, <https://doi.org/10.1007/s00253-012-4439-8>.
- [44] M. Kaasalainen, E. Mäkilä, J. Riikonen, M. Kovalainen, K. Järvinen, Effect of isotonic solutions and peptide adsorption on zeta potential of porous silicon nanoparticle drug delivery formulations, *Int. J. Pharm.* 431 (2012) 230–236, <https://doi.org/10.1016/j.ijpharm.2012.04.059>.
- [45] L. Keawchaon, R. Yoksan, Preparation, characterization and in-vitro release study of carvacrol-loaded chitosan nanoparticles, *Colloids Surf. B Biointerf.* 84 (2011) 163–171, <https://doi.org/10.1016/j.colsurfb.2010.12.031>.
- [46] A.K. Kohli, H.O. Alpar, Potential use of nanoparticles for transcutaneous vaccine delivery: effect of particle size and charge, *Int. J. Pharm.* 275 (2004) 13–17, <https://doi.org/10.1016/j.ijpharm.2003.10.038>.
- [47] D.B. Shenoy, M.M. Amiji, Poly(ethylene oxide)-modified poly(ϵ -caprolactone) nanoparticles for targeted delivery of tamoxifen in breast cancer, *Int. J. Pharm.* 293 (2005) 261–270, <https://doi.org/10.1016/j.ijpharm.2004.12.010>.
- [48] D. Zheng, X. Li, H. Xu, X. Lu, Y. Hu, W. Fan, Study on docetaxel-loaded nanoparticles with high antitumor efficacy against malignant melanoma, *Acta Biochim. Biophys. Sin.* 41 (2009) 578–587, <https://doi.org/10.1093/abbs/gmp045>. Advance.
- [49] C. Wu, T.F. Jim, Z. Gan, Y. Zhao, S. Wang, A heterogeneous catalytic kinetics for enzymatic biodegradation of poly(ϵ -caprolactone) nanoparticles in aqueous solution, *Polymer (Guildf)* 41 (2000) 3593–3597, [https://doi.org/10.1016/S0032-3861\(99\)00586-8](https://doi.org/10.1016/S0032-3861(99)00586-8).
- [50] R. Gul, N. Ahmed, N. Ullah, M.I. Khan, A. Elaissari, A. Rehman, Biodegradable ingredient-based emulgel loaded with ketoprofen nanoparticles, *AAPS PharmSciTech.* 19 (2018) 1869–1881, <https://doi.org/10.1208/s12249-018-0997-0>.
- [51] T.R. Keepers, M. Gomez, C. Celeri, W.W. Nichols, M. Krause, Bactericidal activity, absence of serum effect, and time-kill kinetics of ceftazidime-avibactam against β -lactamase-producing Enterobacteriaceae and *Pseudomonas aeruginosa*, *Antimicrob. Agents Chemother.* 58 (2014) 5297–5305, <https://doi.org/10.1128/AAC.02894-14>.
- [52] J.A. Kamimura, E.H. Santos, L.E. Hill, C.L. Gomes, Antimicrobial and antioxidant activities of carvacrol microencapsulated in hydroxypropyl-beta-cyclodextrin, *LWT - Food Sci. Technol.* 57 (2014) 701–709, <https://doi.org/10.1016/j.lwt.2014.02.014>.
- [53] S. Kalita, B. Devi, R. Kandimalla, K.K. Sharma, A. Sharma, K. Kalita, A.C. Katak, J. Kotoky, Chloramphenicol encapsulated in poly- ϵ -caprolactone – pluronic composite: nanoparticles for treatment of MRSA-infected burn wounds, *Int. J. Nanomed.* 10 (2015) 2971–2984, <https://doi.org/10.2147/IJN.S75023>. eCollection.